Journal of The Electrochemical Society, **159** (3) G23-G28 (2012)
0013-4651/2012/159(3)/G23/6/$28.00 © The Electrochemical Society

The Mechanical Property, Microstructure, and Pore Geometry of a Methyltrimethoxysilane Modified Silica Zeolite (MSZ) Film

Mu-Lung Che, Shindy Chuang, and Jihperng Leu*,z

Department of Materials Science and Engineering, National Chiao Tung University, Hsinchu 30010, Taiwan

A methyltrimethoxysilane (MTMS) modified silica zeolite (MSZ) film has been prepared using a high ratio of MTMS/tetraethyl orthosilicate (TEOS). This study investigated the effect of MTMS addition on the low-*k* matrix structure, elastic modulus, and pore geometry. High MTMS loading reduced the *k*-value of MSZ film down to 2.0, but yielded a lower elastic modulus, 2.7 GPa. Based on grazing-incidence small-angle X-ray scattering (GISAXS) 2D pattern analysis, the pore geometry of the MSZ film was found to be small but elliptical ($R_{in\text{-}plane}$ ~3.75 nm; $R_{out\text{-}of\text{-}plane}$ ~3.04 nm). The elliptical pore shape was formed by a collapse of film structure at 150–160°C as a result of ~32% thickness shrinkage due to the decomposition of tetra-n-propylammonium hydroxide (TPAOH), a structure directing catalyst, and due to a large degree of crosslinking reaction in the silica matrix. Combining GISAXS, ^{29}Si-NMR, and FT-IR results, we propose that the lower elastic modulus was caused by the incorporation of a large amount of methyl groups from the MTMS precursor and the elliptic pores.
© 2012 The Electrochemical Society. [DOI: 10.1149/2.074203jes] All rights reserved.

Manuscript submitted September 29, 2011; revised manuscript received December 9, 2011. Published January 10, 2012.

In order to alleviate the signal delay issue in the backend interconnects as the scaling of the IC devices continues, the search for low-dielectric-constant (low-*k*) interlayer dielectrics remains to be the key materials solution, in addition to 3D interconnects and air-gap approaches.[1] According to 2010 ITRS, upcoming 22 nm technology node of IC industry requires dielectric materials with *k*-value <2.3.[2] Extensive efforts have been made in the last decade to attain ultra-low-*k* dielectrics ($k \sim 2.3$-2.0). Researchers have introduced nanometer-scale pores into spin-on organosilicate dielectric films such as silsesquioxane based materials, whose *k* is ~2.8 to 3.0 and *E* is in ~3 to 7 GPa range at no porosity.[3] However, the mechanical strength of their corresponding ultra-low-*k* materials, which typically have high porosity, ~50-60%, degrades significantly.[4] Moreover, the pore generators (porogens) within the spin-on organosilicate matrix tend to aggregate during the curing step and result in larger pores upon thermal decomposition, which further degrades mechanical strength of the dielectric film.[5] Overall, the mechanical strength of spin-on dielectric films has been a challenge for its use in the manufacturing of advanced integrated circuit.

Recently, researchers have focused on low-*k* films with high mechanical modulus, such as pure silica-zeolite (PSZ) low-*k* film. PSZ low-*k* film offers several advantages over amorphous silica including crystalline structure as well as intrinsically uniform and small pore size.[6,7] Typical PSZ materials have high modulus and low dielectric constant, but have challenges such as high surface roughness,[8] which can be resolved by adding a chemical mechanical polishing step. The other major problem is the high moisture absorption of PSZ film.[9,10] This is disadvantageous for the practicability of PSZ film due to the k-value of water is close to 80. Therefore, there have been some efforts to overcome this problem, for example, by performing fluoro-organic functionalization or silylation using 1H,1H,2H,2H-perfluorooctyltriethoxysilane, 3,3,3-trifluoropropyltrimethoxysilane,[11] trimethylchlorosilane (TMCS), hexamethyldisilazane (HMDS),[12] and/or methyltrimethoxysilane (MTMS)[8,13,14] during the zeolite synthesis and/or during heating processes to make the surface more hydrophobic. One of potential approaches is to develop a silica-zeolite type low-*k* film with low surface roughness and low moisture absorption by packing zeolite particles with only several nanometers and incorporating directly hydrophobic methyl (CH_3) groups such as MTMS. This approach can be represented by nano-clustering silica (NCS), an altered silica-zeolite (MFI-type zeolite) low-*k* material developed by Catalysts & Chemicals Industries Co. Ltd. (currently JGC Catalysts and Chemicals Ltd.).[15] NCS is built up by small silica clusters, which are bounded a small symmetry organic cation that acts as a structure-directing agent (SDA). SDA is predominately consisted of hydrophobic cores with hydrophilic clusters. The hydrophobic core is mainly an alkyl chain, while the hydrophilic cluster is typically a hydrophilic silica matrix. A meso-/micro- porous NCS low-*k* materials can be obtained after thermal curing at high temperature ≥250°C to cross-link silica precursor and remove SDA. NCS film possesses high elastic modulus (10-8 GPa), high hardness (1.0-0.7 GPa), and low dielectric constant (~2.3).[15,16] It has been reported in the literatures that NCS2.3 (NCS film with *k*-value = 2.3) was successfully integrated into the copper/low-*k* interconnects in CMOS 65 nm and 45 nm technology nodes.[17,18]

For future applications in 22 nm node and beyond, it is desirable to further reduce the dielectric constant down to 2.0 based on NCS2.3 with high mechanical strength. In this paper, methyltrimethoxysilane (MTMS) was added as a second component along with tetraethyl orthosilicate (TEOS) to serve as the silica matrix in order to further reduce the dielectric constant.[15] For this, a MTMS modified silica zeolite (MSZ) low-*k* film was prepared and examined using MTMS/TEOS at a ratio of 4.0. The effect of large MTMS loading on the structural parameters such as chemical/molecular bonding, porosity, and pore geometry was investigated. Furthermore, its impact on the MSZ film properties such as mechanical modulus and dielectric constant was examined and discussed.

Experimental

The MSZ precursor was obtained from JGC Catalysts and Chemicals Ltd. which consists of MTMS/TEOS as silica precursor as matrix, tetra-n-propylammonium hydroxide (TPAOH) as the structure directing catalyst (SDC), and solvents (ethanol, water). The SDC/matrix ratio in the MSZ precursor is 1.40, and the MTMS/TEOS ratio is 4.0. For thin-film coating, the solution was initially filtered through a 0.20 μm PTFE filter (Millipore Inc.), and then spun onto a (100) silicon wafer at 2000 rpm for 30 seconds at room temperature. Then a soft-bake at 150°C using a hot-plate was applied for 1 minute to remove the solvent after spin-coating. The film was further cured at 250°C for 10 minutes in a vacuum furnace under a nitrogen purge, then at 400°C for one hour. For all tests except nano-indentation measurement, the nominal thickness of low-*k* films is ~0.3 μm. But, a film thickness of 1 μm is used in order to avoid the substrate effect for the nano-indentation measurement.

The dielectric constant (*k*) of the film was measured using CV-dots test based on a MIS configuration (Al electrode/low-*k* film/Si (10 ohm-cm)) by using a Helwett-Packard 4280A Impedance Analyzer operated at 1 MHz and sweeping from −10V to 10V. The sample was placed under a dry nitrogen purge condition at room temperature. The dielectric constant (*k*) of the films was determined by

* Electrochemical Society Active Member.
z E-mail: jimleu@mail.nctu.edu.tw

Downloaded on 2014-04-28 to IP 140.113.38.11 address. Redistribution subject to ECS terms of use (see ecsdl.org/site/terms_use) unless CC License in place (see abstract).

the following Eq. 1:[3]

$$k = \frac{C}{A} \times \frac{d}{\varepsilon_0} \quad [1]$$

where C is the capacitance of the MIS structure, d is the in film thickness, A is the area of the aluminum dot, ε_0 is the permittivity of free space (8.854×10^{-12} F/m). The elastic modulus (E) of the low-k films was measured using a nanoindenter (MTS, Nano Indenter XP system) with a Berkovich tip in continuous mode based on the Oliver-Pharr method.[19] The density of the low-k film was measured by X-ray reflectivity (XRR). The film was scanned by an X-ray diffracmeter (PANalytical X'Pert Pro MRD) with Cu K_α source ($\lambda = 0.154$ nm) using ω-2θ method with scan angle from 0° to 2°.

The pore geometries (i.e. shape and size) were obtained by grazing-incidence small-angle X-ray scattering (GISAXS) measurements using BL23A beam-line of the National Synchrotron Radiation Research Center (NSRRC) in Taiwan. The incidence beam extracted from a super-conducting wavelength-shifter X-ray source, was monochromated to a wavelength (λ) of 1.55 Å by a Ge(111) double crystal monochromator, with $\Delta\lambda/\lambda \sim 10^{-3}$ resolution. All of the GISAXS data were obtained using an area detector that covered the scattering wave vector (q) ranging from 0.01 to 0.1 $Å^{-1}$, and the incident angle of the X-ray beam (0.5 mm diameter) was fixed at 0.2° with X-ray energy of 10 keV. All GISAXS data were corrected for sample transmission, background, and the detector sensitivity. Then the pore size was analyzed by Guinier's law.[20]

The chemical makeup was examined using Fourier-transform infrared spectroscopy (FT-IR). The measurements were performed using a MAGNA-IR 460 (Nicolet Inc.) in transmission mode with normal incidence angle and 32 scans at a 4 cm^{-1} spectral resolution. The solid-state ^{29}Si NMR (Bruker DSX400WB) was employed to determine the types of silicate structures in the MSZ films. Investigation was focused on Q [$(SiO)_4Si$] structure at −110 ppm and T [$(SiO)_3Si(CH_3)$] structure at −64.5 ppm.

Results And Discussion

Dielectric constant, mechanical modulus, and porosity.— In order to understand the effect of adding large MTMS on the dielectric constant of the MSZ low-k film, the dielectric constant was first investigated. The k-value of MSZ film was measured to be 2.0 by using CV-dots test, as listed in Table I. The porosity of the MSZ low-k film was found to be 38 vol% using XRR measurement. Since the mechanical strength of low-k dielectric thin films is one of the critical properties in backend processing steps such as chemical-mechanical polishing (CMP) and die/packaging interaction,[21] the elastic modulus of MSZ film was also characterized. The elastic modulus of the MSZ low-k film is 2.7 GPa as measured by nanoindentation and listed in Table I, which is much lower than that of NCS2.3 (~10 GPa).[22] The mechanical strength of porous low-k thin films can be affected by several factors such as porosity, pore aggregation or the presence of terminal groups (i.e. CH_3 from MTMS).[23,24] H. Miyoshi et al.[25] proclaimed that porosity is the major factor that affects the modulus. Pore size distribution or pore position is not the main damage responsible for the modulus degradation in porous dielectrics as long as a pore arrangement with no aggregation is achieved. Another dominant factor for the degradation of modulus is the presence of terminal groups.

Table I. Comparison in SDC/Si matrix ratio, mechanical and dielectric properties, and porosity between NCS2.3 and MSZ films.

Sample	SDC/Si matrix ratio	E (GPa)	P (vol%)	k
MSZ	1.40	2.7	38	2.0
NCS2.3[15,16]	–	10-8	29	2.3

E: modulus; P: porosity; k: dielectric constant

S. Eslava et al. reported that their zeolite-inspired low-k (ZLK) film, which possessed 1.0 of MTMS/TEOS ratio, has 6–7 GPa of modulus with ~30 vol% porosity compared to 30–40 GPa of PSZ without MTMS modified.[14,18] In this paper, the MTMS/TEOS ratio of MSZ film is 4.0, which is much higher than 1.0 of ZLK film. Hence, it is predicable that the modulus of MSZ film will be degraded due to the presence of large amount terminal groups. Large amount of MTMS addition may also affect the pore geometry. However, there is still little understanding for the pore geometry of MTMS modified silica zeolite materials. Therefore, in the following sections, we examine the pore geometry (pore size and shape) using GISAXS and other structural factors affecting the modulus of a MSZ film.

Pore geometry of the MSZ low-k film.— Characterization of the pore geometry inside a microporous film only few hundred nanometers thick remains to a challenging task. Although transmission electron microscopy (TEM),[26] positron annihilation spectroscopy (PALS),[27] and ellipsometric porosimetry (EP)[28] have been successfully used in pore size characterization, a non-destructive, grazing-incidence small-angle X-ray scattering (GISAXS) technique can precisely determine and offer complete information of the pore shape, pore sizes, and pore size distribution.[29,30] The two dimensional (2D) GISAXS scattering pattern for MSZ low-k film cured at 400°C is shown in Figure 1. An isotropic, well defined ring of maxima scattering pattern was observed, indicating the existence of randomly distributed pores with narrow pore size distribution. In addition, there was no pore correlation, as illustrated in the scattering pattern.[31]

The scattering patterns were further analyzed by the following GISAXS model to examine their pore geometries. It is known that the intensity of scattering pattern ($I_{(q)}$) is proportional to the product of intra-particle structure factor ($P_{(q)}$, form factor) and inter-particle structure factor ($S_{(q)}$, structure factor) as expressed by Eq. 2:[32]

$$I_{(q)} \propto P_{(q)} \cdot S_{(q)} \quad [2]$$

where q is the scattering wave vector defined by scattering angle (θ) and wavelength of radiation (λ) of X-ray by Eq. 3:

$$q = \frac{4\pi}{\lambda} \cdot \sin\theta \quad [3]$$

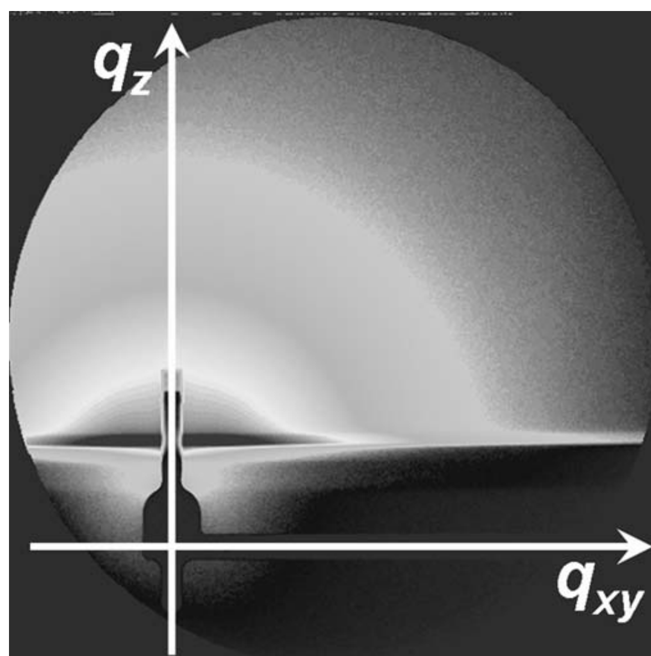

Figure 1. GISAXS 2-D scattering pattern of the MSZ film cured at 400°C.

Downloaded on 2014-04-28 to IP 140.113.38.11 address. Redistribution subject to ECS terms of use (see ecsdl.org/site/terms_use) unless CC License in place (see abstract).

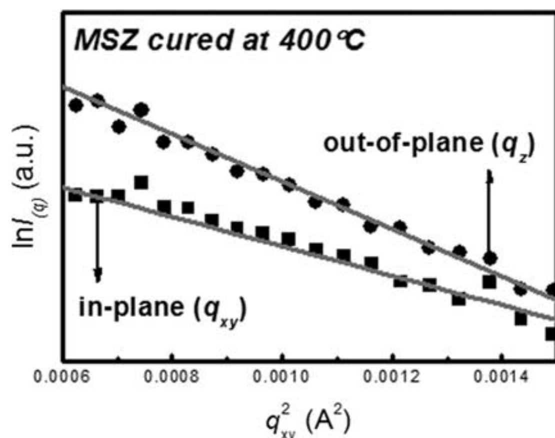

Figure 2. GISAXS 1-D analysis, Guinier plot (ln $I_{(q)}$ vs. q^2) for the MSZ film cured at 400°C.

The structure factor $S_{(q)}$ is close to one in a low-concentration system or a system without inter-particle interactions, and thus can be ignored. Hence, the scattering intensity distribution for a polydisperse system is proportional to the ensemble average of the form factor ($P_{(q)}$) which has been evaluated for a variety of particle shapes (spheres, rods, disks etc.). However, in the range of very low q-value ($q \ll 1$), $P_{(q)}$ can be generalized for a spherical particle system by using the Guinier approximation with a radius of gyration (R_g), and then Eq. 3 can be further derived as Eq. 4:

$$I_{(q)} \propto \exp\left(\frac{-q^2 R_g^2}{3}\right) \qquad [4]$$

Hence, a linear relationship exists between ln$I_{(q)}$ and q^2, with a slope of ($-R_g{}^2/3$), and the steeper the slope, the larger the radius.

Figure 2 shows the Guinier plot (ln$I_{(q)}$ vs. q^2) for MSZ film cured at 400°C, which were extracted from MSZ film scattering pattern and approximated by Guinier theory for quantitative analysis. There are two slopes can be found for in-plane (q_{xy} direction) and out-of-plane (q_z direction) of the MSZ film cured at 400°C, respectively. Since the slope is related to the gyration radius (R_g) of pores in the low-k matrix, the pore radii of the pores in MSZ film were found to be quite different in two different directions. In Guinier plot, slope in the in-plane direction is −282.0 Å^2, which is steeper than the slope in the out-of-plane direction, −185.4 Å^2. Thus, $R_{g,in\text{-}plane}$ is 2.91 nm and $R_{g,out\text{-}of\text{-}plane}$ is 2.36 nm.

Based on Guinier theory, the radius of pore size (R) can be deduced from the following expression, Eq. 5:[33]

$$R = \sqrt{\frac{5}{3}} \times R_g \qquad [5]$$

Thus, the radius in the in-plane direction (R_{IP}) is calculated to be 3.75 nm, while the radius in the out-of-plane direction (R_{OP}) is 3.04 nm.

GISAXS data shows that the elliptical pores were formed in the MSZ matrix with the long axis parallel to the substrate. However, the formation mechanism of such elliptical pores is not yet understood, though it is important for tailoring the mechanical properties of MSZ film. Therefore, in situ GISAXS measurements of the MSZ films as a function of cure temperature from 150 to 400°C were carried out in order to understand the evolution of SDC/pore shape and size. Figures 3a–3c show the GISAXS 2-D patterns of the MSZ film cured at 150°C, 250°C, and 400°C, respectively. The scattering patterns for MSZ film cured at various cure temperatures maintained a similar isotropic ring. This indicates that there is no drastic pore rearrangement such as porogen aggregation, but it cannot distinguish any delicate changes on pore size and shape. Therefore, similar 1-D Guinier analysis was carried out to determine any change of pore radius in the in-plane and out-of-plane directions compared to as the aforementioned MSZ film cured at 400°C. Figure 4a shows that the in-plane slope of MSZ film decreased from −270.4 Å^2 to −279.0 Å^2, then −282.0 Å^2 when the curing temperature was increased from 150°C, 250°C, then 400°C. Figure 4b shows that the out-of-plane slope increased from −233.6 Å^2 to −202.3 Å^2, then −185.4 Å^2. According to 1-D Guinier analysis and calculation, the pore radii in the in-plane (R_{IP}) and out-of-plane (R_{OP}) directions for the MSZ films cured at various temperatures are summarized in Table II. At 150°C, the R_{IP} and R_{OP} values of the MSZ films were 3.68 nm and 3.42 nm, respectively. The R_{OP}/R_{IP} ratio of 0.93 for MSZ film cured at 150°C indicates that an approximately spherical second phase (silica clusters or pore structure) was formed inside the MSZ matrix. The nature of the second phase is further examined by FT-IR analysis in the

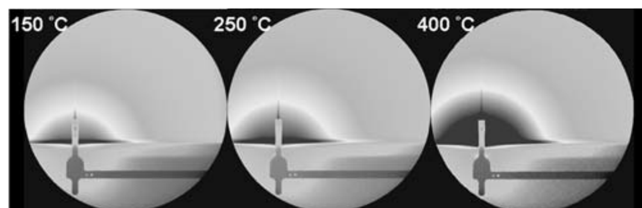

Figure 3. The successive GISAXS 2-D scattering patterns of the MSZ film cured at 150°C, 250°C, and 400°C.

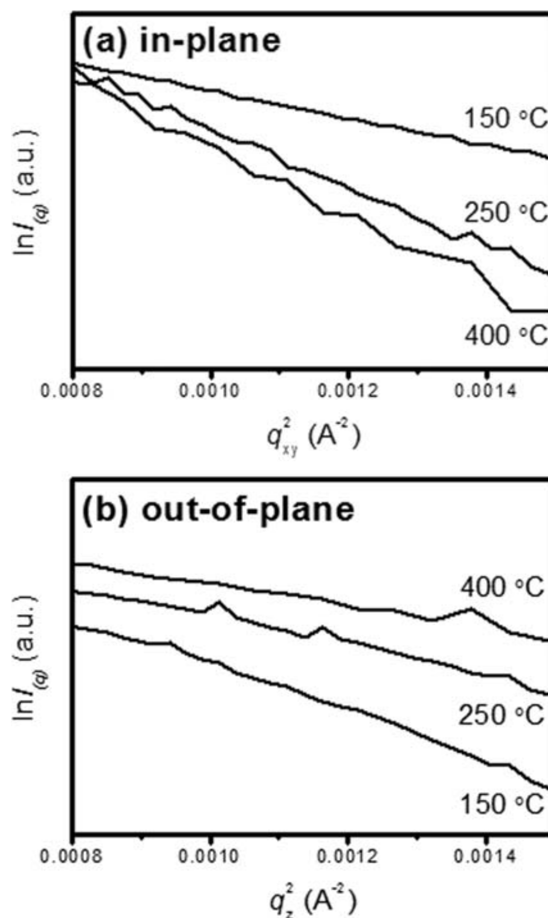

Figure 4. The Guinier plot (ln $I_{(q)}$ vs. q^2) for (a) in-plane and (b) out-of-plane direction of the MSZ films cured at 150°C, 250°C, and 400°C.

Downloaded on 2014-04-28 to IP 140.113.38.11 address. Redistribution subject to ECS terms of use (see ecsdl.org/site/terms_use) unless CC License in place (see abstract).

Table II. The Guinier analysis of GISAXS scattering patterns for the MSZ films cured at 150, 250, and 400°C.

Curing Temperature	R_{IP} (nm)	R_{OP} (nm)	R_{OP}/R_{IP} ratio	Shape
150°C	3.68	3.42	0.93	Spherical
250°C	3.73	3.18	0.85	
400°C	3.75	3.04	0.81	Elliptic

R_{IP}: radius of in-plane direction; R_{OP}: radius of out-of-plane direction

following section. When the curing temperature was raised to 250 and 400°C, the R_{IP} increased from 3.68 nm to 3.73 and 3.75 nm (1.4-1.9% increase), respectively. In contrast, the R_{OP} instead decreased from 3.42 nm to 3.18 nm and 3.04 nm, respectively (i.e. 7-11% reduction). As a result, the R_{OP}/R_{IP} ratio dropped from 0.93 to 0.85-0.81, indicating an elliptical pore shape was formed at $T \geq 250$°C. So far, the porogen or pore structure has been demonstrated to evolve from an approximately spherical shape at 150°C to the elliptic shape at 250°C and above. In specific, the pore radius in the out-of-plane direction shrank up to 11%, leading to an elliptical pore with the longer radius directed parallel to the substrate.

Characterization of MSZ thin-film structure.— Next, we investigated the chemical structure of MSZ film upon the addition of MTMS to TEOS and its structural evolution as a function of cure temperature from 150°C to 400°C. In this study, FT-IR was used to examine the microstructure of MSZ film at various cure temperatures, as shown in Figure 5a. For an as-deposited MSZ film, two characteristic peaks were related to the structure-directing catalyst, TPAOH.[34] A C-H stretching band of CH_x group ($x = 2 \sim 3$) from the alkyl chain of TPAOH located around 2850–3000 cm^{-1}. Another characteristic peak at 1641 cm^{-1}, which between C=N stretching (1690–1640 cm^{-1}) and C-N stretching (1250–1020 cm^{-1}), was speculated to be a C-N^+ stretching peak.[35] Two bands disappeared after curing at 160°C, indicating that the MSZ film became a porous structure upon the decomposition of TPAOH around 160°C.

Furthermore, three major peaks related to Si-CH_3 in the MSZ matrix involve a methyl group (CH_3) deformation peak at 1274 cm^{-1} and Si-C stretching of $Si(CH_3)_x$ ($x = 1 \sim 2$) peaks at 778 cm^{-1} and 849 cm^{-1}. In addition, there are two Si-O-Si stretching absorption bands between 1135 cm^{-1} and 1030 cm^{-1}; namely 1126 cm^{-1}, attributed to a cage-like Si-O-Si structure, and 1028 cm^{-1}, assigned to a network Si-O-Si structure.[36] The network/cage structural ratio was found to increase from 1.32 to 1.88 as cure temperature was raised from 150 to 400°C, as shown in Figure 5b. High curing temperature transformed the cage Si-O-Si structure into higher fraction of network Si-O-Si structure in the MSZ film, thus increasing the degree of crosslinking of MSZ matrix.[37]

In addition, the skeleton structure of matrix may be affected by any film shrinkage during the thermal processes. Figure 6a shows the film thickness and network/cage structural ratio of the MSZ film as a function of cure temperature between 25 and 400°C. In order to analyze their changes in relative scale, the degree of crosslinking was assumed 0% for as-deposited film and 100% crosslinking for the MSZ film cured at 400°C 1 hour. Excellent correlation was found between the film shrinkage trend and the degree of crosslinking in of the MSZ films. Up to 150°C, most of the film thickness reduction (~32%) came from solvent evaporation because the degree of crosslinking increased by only 9%. Between 150–160°C, further film shrinkage from 440 nm to 324 nm (26% reduction) was presumably caused by the decomposition of TAPOH and the crosslinking reaction through polycondensation of silanol groups as the degree of crosslinking jumped from 9% to 70%. Above 160°C, the change rate of the degree of crosslinking was much reduced because the mobility of silica clusters was restricted after the removal of solvents and TPAOH and >70% degree of crosslinking. The same trend

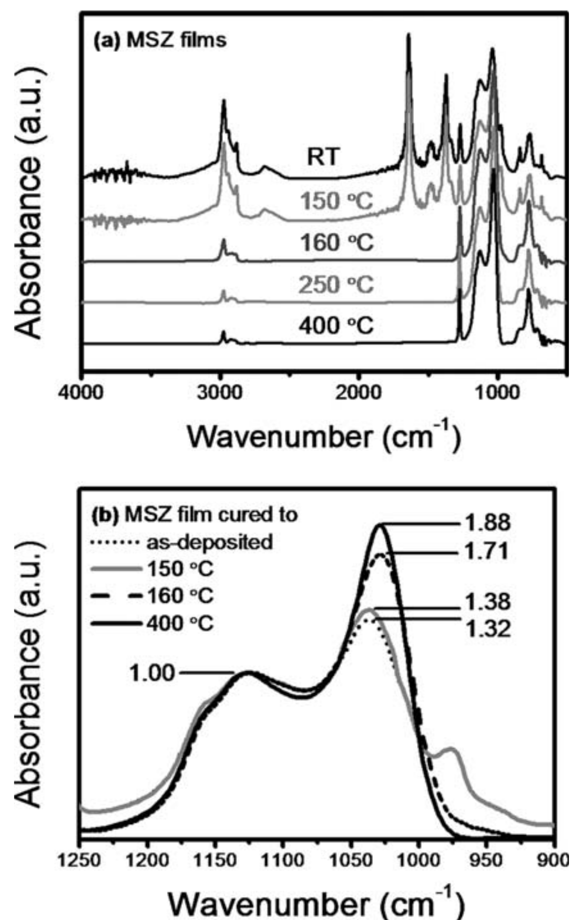

Figure 5. Transmission FT-IR spectra of the MSZ films cured at various temperatures: (a) 500-4000 cm^{-1} and (b) 900-1250 cm^{-1}.

was found in the film thickness variation, where most of the shrinkage occurred at 150-160°C, and there was little change in the film thickness between 160 and 400°C. Overall, MSZ film shrank 32% from 440 nm to 299 nm in the 150–400°C temperature range, a shrinkage that is much larger than that of NCS2.3 (<15%) in 25–400°C range.[38] To sum up, the porous structure was formed upon the decomposition of TPOAH at 160°C. It is postulated that, at this temperature, the large film shrinkage in MSZ film results in high compressive stress and then the collapse of the matrix skeleton,

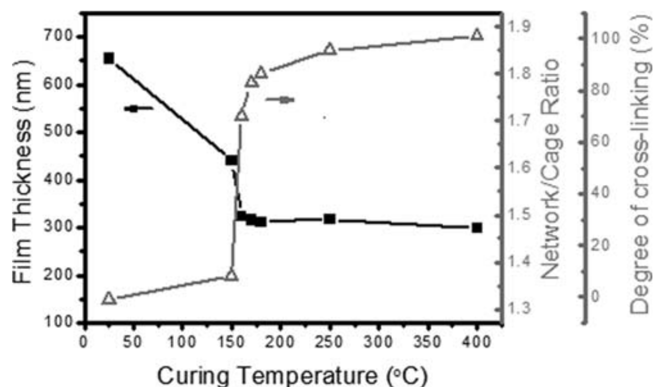

Figure 6. The film thickness, network/cage structural ratio and the degree of cross-linking of the MSZ film as a function of cure temperature between 25 and 400°C.

Downloaded on 2014-04-28 to IP 140.113.38.11 address. Redistribution subject to ECS terms of use (see ecsdl.org/site/terms_use) unless CC License in place (see abstract).

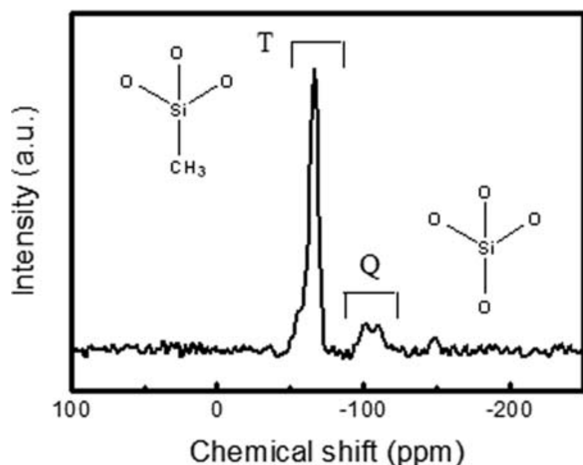

Figure 7. ^{29}Si NMR spectrum for the MSZ low-*k* film cured at 400°C.

thereby transforms the pores from approximately spherical to elliptical.

The matrix skeleton of MSZ film cured at 400°C, especially the actual MTMS (or CH_3) amount in the MSZ low-*k* film can be measured by ^{29}Si NMR spectroscopy. Figure 7 shows a predominant T-structure $[(SiO)_3Si(CH_3)]$ and a minor Q-structure $[(SiO)_4Si]$ in the MSZ samples. The Q-group, which is a fully cross-linked Si-O-Si structure,[39] originates from TEOS, while T-group comes from MTMS. NMR spectrum shows the T/Q structural ratio is close to 4.0, which is consistent with the MTMS/TEOS ratio in the MSZ solution. Overall, dense oxide consisted of a network of tetrahedral Si-O bonding obtained through the hydrolysis of TEOS monomer. Introducing Si-CH_3 bonds in MTMS resulted in matrix formation with only three Si-O bonds and less cross-linking. Therefore, the minor amount of Q-group and predominant T-group revealed a relatively loose microstructure in the MSZ skeleton compared with conventional NCS2.3 film. The less cross-linked structure may contribute the degradation of the mechanical modulus of MSZ films beyond the scaling of modulus by the incorporation of porosity. For the same reason, the MSZ low-*k* film may not sustain the stress developed by the crosslinking reaction at 150–160°C and the film shrinkage due to the decomposition of TAPOH. As a result, the MSZ film collapses and yields an elliptical pore structure, which weakens the film's mechanical strength compared to an isotropic, spherical pore.

For ultra-low-*k* MSZ film, the incorporation of methyl groups such as MTMS terminal may reduce the dielectric constant. However, the tradeoff is the degradation of elastic modulus beyond the scaling of volume porosity if there is an excess of terminal Si-CH_3 groups and deviation from spherical pore shape. Therefore, it is important to optimize the thermal curing profile while minimizing film thickness shrinkage in order to obtain approximately spherical pores without degrading the mechanical strength at a fixed MTMS/TEOS ratio.

Formation mechanism on the elliptic pores.— Finally, based on the above discussions, we propose a formation mechanism of the elliptical pores in MSZ film. Similar to general NCS low-*k* film,[15] the pores in MSZ low-*k* film are generated from structure directing catalyst, TPAOH, which can be decomposed and removed after a high-temperature curing process. Due to its amphiphilic characteristics with a long alkyl chain in the hydrophobic end, TPAOH forms a micelle structure when it is mixed with another hydrophilic precursor, like silica precursor (TEOS or MTMS), and solvents. These micelles are also called clusters for the nano-clustering silica films, as shown in Figure 8a. As the curing temperature is increased to 150°C (soft-baking), the solvent is fully removed, resulting in ∼32% (from 650 nm to 440 nm) film thickness reduction. In this stage, the MSZ film is still soft due to the presence of TPAOH and a limited degree of cross-linking (∼9%). Thus, there is no compressive force induced by structural transformation to affect the TPAOH micelle shape as schematically illustrated in Figure 8b. The approximately spherical TPAOH micelle structure ($R_{OP}/R_{IP} = 0.93$) has been quantified by GISAXS analysis.

When curing temperature is increased to near the decomposition temperature of TPAOH, i.e. 150∼160°C as shown in Figure 8c, the mesopores are formed through the packing of clusters inside the amorphous silica matrix.[40] In this stage, there is a higher probability for silica clusters to come closer and form more Si-O-Si network structure. At 160°C, the degree of crosslinking jumps to ∼70% along with the loss of TPOAH, making the MSZ matrix rigid. At the same time, shrinkage of film thickness places a compressive stress on the MSZ skeleton. If the matrix has enough mechanical strength to sustain the compressive stress, the pore shape will not be changed. However, the silica matrix of the MSZ has a relatively weak skeleton due to a high percentage of terminal groups when a MTMS/TEOS ratio of 4.0 is introduced in the low-*k* precursor. As a result, the MSZ skeleton cannot sustain the compressive stress, so the film pore shape is compressed from spherical to ellipsoidal after curing at T ≥160°C, as illustrated in Figure 8d.

Conclusions

An ultra-low-*k* film, modified silica zeolite (MSZ), with $k = 2.0$ has been prepared using a ratio of MTMS/TEOS of 4. The effect of MTMS addition on the low-*k* matrix structure, elastic modulus, and pore geometry has been examined in this study. High MTMS loading reduced the *k*-value down to 2.0, but yielded a lower elastic modulus of MSZ film, 2.7 GPa. Based on GISAXS 2D pattern using Guinier approximation, the pore geometry of the MSZ film was found to be small but elliptical ($R_{in\text{-}plane} \sim 3.75$ nm; $R_{out\text{-}of\text{-}plane} \sim 3.04$ nm). The formation mechanism of elliptical pores was proposed. The elliptical pore shape was formed by a collapse of film structure at 150–160°C as a result of ∼32% thickness shrinkage due to the decomposition of

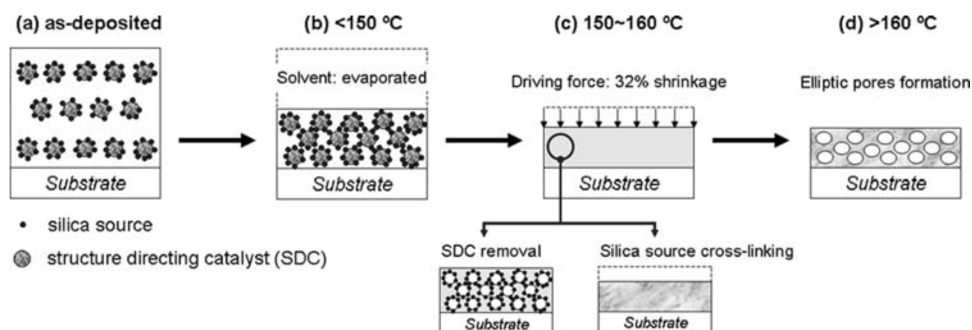

Figure 8. Schematic diagrams for the formation mechanism of the elliptical pores in the MSZ low-*k* film.

Downloaded on 2014-04-28 to IP 140.113.38.11 address. Redistribution subject to ECS terms of use (see ecsdl.org/site/terms_use) unless CC License in place (see abstract).

TPAOH and a large degree of crosslinking reaction in the silica matrix. Combining GISAXS, ^{29}Si-NMR, and FT-IR results, we proposed that the lower elastic modulus was caused by the incorporation of a large amount of methyl groups from the MTMS precursor and the elliptical pores.

Acknowledgments

The authors at NCTU thank Dr. U-Ser Jeng of NSRRC for his assistance in the GISAXS measurements. The authors also thank the financial support in part by JGC Catalysts & Chemicals Ltd. and National Science Council (Taiwan) under Contract Nos. NSC98-2221-E-009 -177 and NSC 99-2221-E-009 -177.

References

1. M. T. Bohr, *Tech. Digest IEEE Int. Electronic Device Meeting*, 241 (1995).
2. *International Technology Roadmap for Semiconductor*, Executive Summary, 2010 Edition (2010).
3. P. S. Ho, J. Leu, and W. W. Lee, *Low Dielectric Constant Materials for IC Applications*, Springer, New York, (2002).
4. K. Maex, M. R. Baklanov, D. Shamiryan, F. Iacopi, S. H. Brongersma, and Z. S. Yanovitskaya, *J. Appl. Phys.*, **93**(11), 8793 (2003).
5. F. Ciaramella, V. Jousseaume, S. Maitrejean, M. Verdier, B. Remiat, A. Zenasni, and G. Passemard, *Thin Solid Films*, **495**, 124 (2006).
6. Z. Li, M. C. Johnson, M. Sun, E. T. Ryan, D. J. Earl, W. Maichen, J. I. Martin, S. Li, C. M. Lew, J. Wang, M. W. Deem, M. E. Davis, and Y. Yan, *Angew. Chem.-Int. Edit.*, **118**, 6477 (2006).
7. Z. Li, S. Li, H. Luo, and Y. Yan, *Adv. Funct. Mater.*, **14**, 1019 (2004).
8. S. Eslava, C. E. A. Kirschhock, S. Aldea, M. R. Baklanov, F. Iacopi, K. Maex, and J. A. Martens, *Microporous Mesoporous Mat.*, **118**, 458 (2009).
9. S. Eslava, F. Iacopi, M. R. Baklanov, C. E. A. Kirschhock, K. Maex, and J. A. Martens, *J. Am. Chem. Soc.*, **129**, 9288 (2007).
10. S. Eslava, S. Delahaye, M. R. Baklanov, F. Iacopi, C. E. A Kirschhock, K. Maex, and J. A. Martens, *Langmuir*, **24**, 4894 (2008).
11. C. M. Lew, Z. Li, S. Li, S. Hwang, Y. Liu, D. I. Medina, M. Sun, J. Wang, M. E. Davis, and Y. Yan, *Adv. Funct. Mater.*, **18**, 3454 (2008).
12. C. M. Lew, Y. Liu, B. Day, G. M. Kloster, H. Tiznado, M. Sun, F. Zaera, J. Wang, and Y. Yan, *Langmuir*, **25**, 5039 (2009).
13. S. Li, Z. Li, D. Medina, C. Lew, and Y. Yan, *Chem. Mater.*, **17**, 1851 (2005).
14. S. Eslava, J. Urrutia, A. N. Busawon, M. R. Baklanov, F. Iacopi, S. Aldea, K. Maex, J. A. Martens, and C. E. A. Kirschhock, *J. Am. Chem. Soc.*, **130**, 17528 (2008).
15. M. Egami, *Science and Industry*, **77**(11), 582 (2003).
16. K. Ito, R. S. Yu, K. Sato, K. Hirata, Y. Kobayashi, T. Kurihara, M. Egami, H. Arao, A. Nakashima, and M. Komatsu, *J. Appl. Phys.*, **98**(9), 094307 (2005).
17. T. Suzuki, I. Sugiura, S. Sato, and T. Nakamura, *Jpn. J. Appl. Phys.*, **43**(5A), L614 (2004).
18. W. Volksen, R. D. Miller, and G. Dubois, *Chem. Rev.*, **110**, 56 (2010).
19. W. C. Oliver and G. M. Pharr, *J. Mater. Res.*, **7**, 1564 (1992).
20. A. Guinier and G. Fournet, *Small Angle Scattering of X-Rays*, John Wiley, New York (1955).
21. J. Tan, Z. W. Zhong, and H. M. Ho, *Microelectron. Eng.*, **81**, 75 (2005).
22. C. Gaire, T. Ou, H. Arao, M. Egami, A. Nakashima, R. C. Picu, G.-C. Wang, and T.-M. Lu, *J. Porous Mater.*, **17**, 11 (2010).
23. N. Aoi, T. Fukuda, and H. Yanazawa, *Proc. Int. 2002 Interconnect Technology Conf., California*, 72, IEEE Press, New Jersey, (2002).
24. H. Miyoshi, H. Matsuo, H. Tanaka, K. Yamada, Y. Oku, S. Takada, N. Hata, and T. Kikkawa, *Jpn. J. Appl. Phys.*, **44**, 1161 (2005).
25. H. Miyoshi, H. Matsuo, Y. Oku, H. Tanaka, K. Yamada, N. Mikami, S. Takada, N. Hata, and T. Kikkawa, *Jpn. J. Appl. Phys.*, **43**, 498 (2004).
26. W. Wu, W. E. Wallace, E. K. Lin, G. W. Lynn, C. J. Glinka, E. T. Ryan, and H. M. Ho, *J. Appl. Phys.*, **87**, 1193 (2000).
27. D. W. Gidley, W. E. Frieze, T. L. Dull, J. Sun, A. F. Yee, C. V. Nguyen, and D. Y. Yoon, *Appl. Phys. Lett.*, **76**, 1282 (2000).
28. M. R. Baklanov and K. P. Mogilnikov, *Microelectron. Eng.*, **64**, 335 (2002).
29. B. Lee, Y. H. Park, Y. T. Hwang, W. Oh, J. Yoon, and M. Ree, *Nature Mater.*, **4**, 147 (2005).
30. B. Lee, J. Yoon, W. Oh, Y. Hwang, K. Heo, K. S. Jin, J. Kim, K. W. Kim, and M. Ree, *Macromolecules*, **38**, 3395 (2005).
31. V. Jousseaume, G. Rolland, D. Babonneau, and J. P. Simon, *Thin Solid Films*, **517**, 4413 (2009).
32. S. W. Yeh, K. H. Wei, Y. S. Sun, U. Jeng, and K. S. Liang, *Macromolecules*, **38**(15), 6559 (2005).
33. L. A. Feigin and D. I. Svergun, *Structure Analysis by Small Angle X-ray and Neutron Scattering*, Plenum, New York (1987).
34. SDBSWeb : http://riodb01.ibase.aist.go.jp/sdbs/ (National Institute of Advanced Industrial Science and Technology, Japan, 07.20.2011), SDBS No.: 21711.
35. D. L. Pavia and G. M. Lampman, *Introduction to Spectroscopy*, 4th edition, Cengage Learning, United State (2009).
36. C. Y. Wang, Z. X. Shen, and J. Z. Zheng, *Appl. Spectrosc.*, **54**, 209 (2000).
37. L. Lee, W. Chen, and W. Liu, *J. Polym. Sci. Pol. Chem.*, **40**, 1560 (2002).
38. T. Owada, N. Ohara, H. Watatani, T. Kouno, H. Kudo, H. Ochimizu, T. Sakoda, N. Asami, Y. Ohkura, S. Fukuyama, A. Tsukune, M. Nakaishi, T. Nakamura, Y. Nara, and M. Kase, *2009 Proc. Int. Interconnect Technology Conf.*, 149, IEEE Press, (2009).
39. S. Kim, Y. Toivola, R. F. Cook, K. Char, S. H. Chu, J. K. Lee, D. Y. Yoon, and H. W. Rhee, *J. Electrochem. Soc.*, **151**, F37 (2004).
40. T. Nakamura and A. Nakashima, *2004 Proc. Int. Interconnect Technology Conf.*, 175, IEEE Press, (2004).

Downloaded on 2014-04-28 to IP 140.113.38.11 address. Redistribution subject to ECS terms of use (see ecsdl.org/site/terms_use) unless CC License in place (see abstract).